Corrosion inhibitors for carbon steel N80 in an acidic medium by using the compound (*E*)-*N*-(benzo[*d*]thiazol-2-yl)-1-(2,3-dihydrobenzo[*b*][1,4]dioxin-6-yl)methanimine

A.M. Jabbar* and A.S. Abdulnabi

Chemistry Department, Education College for Pure Sciences, Basrah University, Basrah 61001, Iraq
**E-mail: abmohammed2341992@gmail.com*

Abstract

A new heterocyclic organic corrosion inhibitor, the Schiff base [*N*-(benzo[*d*]thiazol-2-yl)-1-(2,3-dihydrobenzo[*b*][1,4]dioxin-6-yl)methanimine], has been prepared by reflux distillation. Its properties have been analyzed by means of FT-IR, UV-Vis, ^{1}H NMR, ^{13}C NMR, EI-Mass, SEM and EDS spectroscopic techniques. This synthesized chemical was used as a corrosion inhibitor in our study at various concentrations (0.0001, 0.0005, 0.001, and 0.005 M) and temperatures (298, 308, and 318 K) on carbon steel N80 in 1 M HCl and was studied by potentiodynamic polarization methods (Tafel plots). The findings proved that with an increase in concentration and temperature of the inhibitor, the percentage of inhibition efficiency (%*IE*) elevates. The most excellent corrosion inhibition efficiency of 95.71% was reached at 0.005 M at 318 K in 1 M HCl. The results of Sh_1 as a corrosion inhibitor indicated that the adsorption of the inhibitor on the surface of carbon steel was of physisorption type and obeyed the Langmuir adsorption isotherm. Accordingly, we also studied the activation energy, and thermodynamic parameters were calculated from the Langmuir adsorption isotherm, including the free energy ΔG^0, enthalpy ΔH^0, and entropy change ΔS^0. This electrochemical method (Tafel extrapolation) along with SEM and EDS techniques confirmed that this prepared inhibitor protects carbon steel from corrosion by forming a film (protection layer) on its surface.

Received: January 19, 2024. Published: June 7, 2024 doi: 10.17675/2305-6894-2024-13-2-27

Keywords: *Schiff base, Tafel plot, adsorption isotherm, physisorption, Langmuir equation.*

1. Introduction

Mild steel (MS) is frequently used in many industrial sectors, such as pipeline construction and acid pickling, due to its availability and excellent mechanical and physical characteristics [1]. In corrosive media, carbon steel corrosion occurs through chemical/electrochemical reactions between the metals and the aggressive environment. To minimize corrosive attacks on metallic materials, the application of corrosion inhibitors to protect metals from corrosion appears to be the most effective method of metal protection [2]. Thus, the inhibitors can be defined are substances used to prevent or reduce metal surface corrosion in corrosive environments [3] and they are among the types of protective measures

proposed against the corrosion process. An inhibitor is a chemical that significantly reduces the corrosion rate when added to the corrosion medium in a low concentration [4, 5] and inhibits corrosion by adsorption; thus, inhibitors that can adsorb on metal surfaces will impede such metal's dissolution or corrosion reaction in the corrosive medium and protect it by creating a film on the metal surface [6]. Effective organic inhibitors with triple bonds, conjugated double bonds, and resonance rings of aromatic and hetero atoms (oxygen, sulfur, and nitrogen) in their structures act as corrosion inhibitors [7, 8]. The adsorption of a molecule on a metal surface depends on the polar function of the molecule [9]. These inhibitors work against metallic corrosion in acid and basic environments. Cyclic and non-cyclic nitrogen compounds are effective inhibitors against corrosion of mild steel in acid solutions [10]. The mechanism of dissolution of iron in an acid chloride medium can be represented [11] as follows:

$$Fe + Cl^- \longleftrightarrow FeCl^-_{ads}$$
$$FeCl^-_{ads} \longleftrightarrow FeCl^+_{ads} + 2e^-$$
$$FeCl^+_{ads} \longleftrightarrow Fe^{+2} + Cl^-$$

Schiff bases are organic compounds that demonstrated their power against steel corrosion in acid media resulting from the presence of their adsorptive –HC=N-group exhibiting a lone pair of electrons on nitrogen atoms and a planar structure; they are easily synthesizable by condensation of primary amines and carbonyl compounds [12]. Current studies show that numerous organic inhibitors are adsorbed on the outer part of a metal surface by expelling water molecules from the outer surface and creating a dense film wall. The presence of a lone electron pair and π-electrons in the inhibitor molecules leads to acceleration of the process of electron transfer from the inhibitor to the metal, and thus, a coordinate covalent bond is formed responsible for transferring electrons from the inhibitor to the outer surface of the metal [13].

2. Materials and Instruments

The chemical products utilized in the experiment were: 2-aminobenzothiazol (analytical quality) from Merk Company; 1,4-benzodioxane-6-carboxaldehyde was from Alfa Aesar Company; and the other chemical compounds were from Sigma. In all of them, the purity was 99%, and these were used in the preparation. The alloy utilized to investigate the corrosion process was carbon steel N80; the weight percentage of its constituents were: C 4.97%, Si 0.29%, Au 12.15%, O 2.02, and Fe 80.57%. The FT-IR analysis of the synthesized compounds was performed at room temperature utilizing a Japanese-made Shimadzu 8400S with potassium bromide disks at 400–4000 cm^{-1}. The analysis of the UV-visible spectrum was carried out using the Japan PD-303 spectrometer. ^1H and ^{13}C NMR spectrum analysis was performed using Bruker 400 MHz and 100 MHz spectrometers, respectively. Tetramethylsilane (TMS) was used as the internal reference, and DMSO was the solvent. The chemicals' mass spectra were captured using an Agilent Technologies 5975C mass

spectrometer (EI, 70 eV). Scanning electron microscopy (SEM) was used to study the surface morphology of the alloy utilizing the MIRA3 TESCAN device. Energy Dispersive X-ray spectroscopy (EDS) was used to evaluate alloy components utilizing the Oxford instrument device.

3. Synthesis of the Schiff Base

The Schiff base was prepared by the reaction of 1,4-benzodioxane-6-carboxaldehyde with 2-aminobenzothiazole under reflux conditions [14]. The reaction was performed by mixing 0.006 mole (0.9849 g) of 1,4-benzodioxane-6-carboxaldehyde dissolved in ethanol (12 ml) in a round flask of 100 ml capacity with 0.006 mole (0.9012 g) of 2-aminobenzothiazole dissolved in ethanol (12 ml), followed by addition of 3 drops glacial acetic acid. The mixture was refluxed for 22 hours while observing via TLC (*n*-hexane: ethyl acetate/60:40). The product forming a dark yellow crystalline precipitate was filtered off, washed, and parched to get the compound (Sh_1). It was recrystallized from hot tetrahydrofuran (THF) to obtain the product in its pure form (melting point 179–182°C, 72% yield) as illustrated at Figure 1.

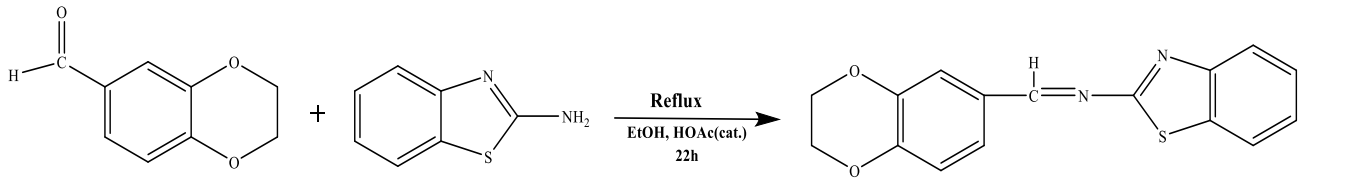

Figure 1. Sh_1 preparation steps.

4. Results and Discussion

4.1. Chemistry

1.FT-IR, UV-Vis, ^{1}H NMR, ^{13}C NMR, and EI-Mass spectroscopy analysis

Several techniques were used to confirm the prepared compound, including FT-IR, UV-Vis, ^{1}H NMR, ^{13}C NMR, and EI-Mass spectroscopy. The FT-IR (KBr, cm^{-1}) spectrum of this compound (Sh_1) shows strong bands at 1649.14 cm^{-1} (C=N of azomethine group), 1587.42 cm^{-1} (C=N ring), 1436.97–1533.41 cm^{-1} (C=C ring), 3059.10–3130.47 cm^{-1} (C–H aromatic) and 3059.10–3130.47cm^{-1} (C–H aliphatic) [15, 16], Figure 2. The UV-Vis spectrum of compound (Sh_1) shows an absorption band at [219.5–286.0] and 339.5 nm as a result of electronic transitions π-π* (aromatic ring) and *n*-π* of (C=N) group, respectively [17], Figure 3. ^{1}H NMR spectrum data: 9.67 ppm [s, 1H, N=CH], 6.76–8.94 ppm [m, 7H, aromatic ring] and 3.07 ppm [d, 4H, $-O-CH_2$], Figure 4. ^{13}C NMR spectrum: 30.88 ppm (methyl carbon), 111.53–166.33 ppm [aromatic carbon], 166.87 ppm [–C=N Schiff] and 172.99 ppm [–C=N ring], Figure 5. MS [EI, *m/z* (%)]: 295.4 (M^+, 150) [18], Figure 6.

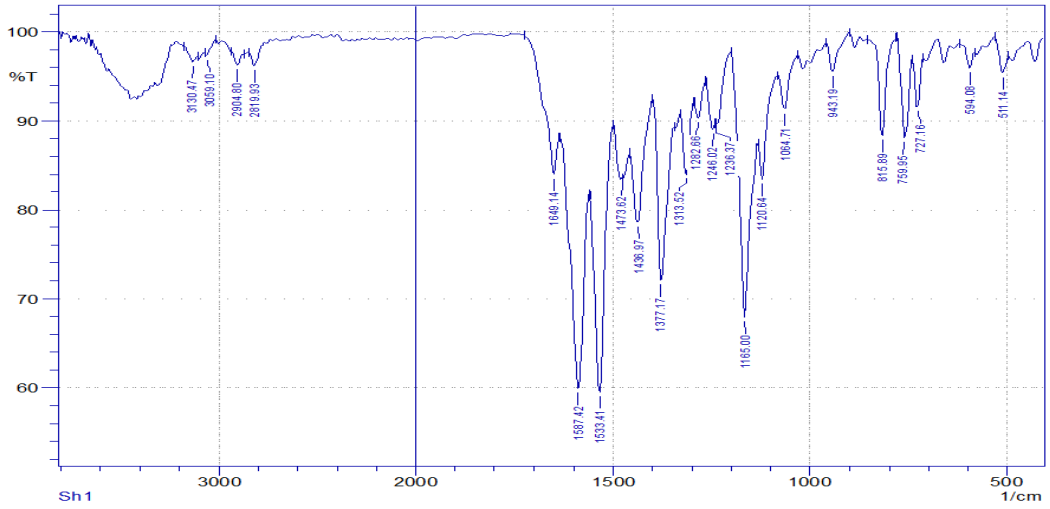

Figure 2. FT-IR spectrum of the Sh_1 molecule.

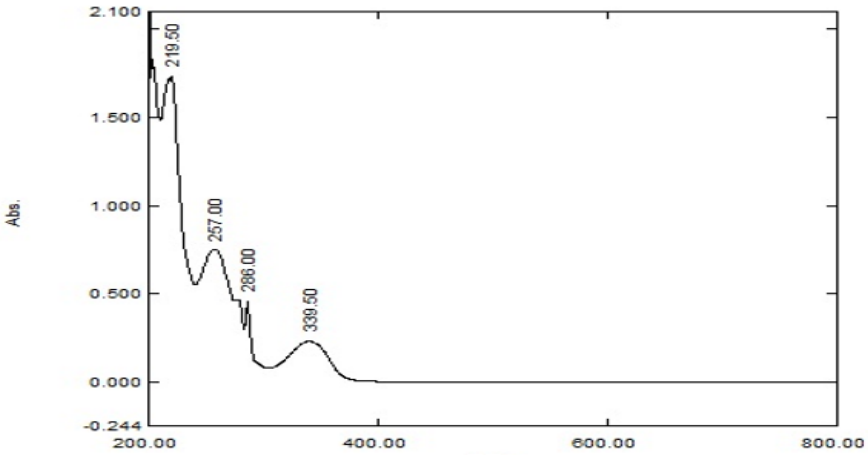

Figure 3. UV-Vis spectrum of the Sh_1 molecule.

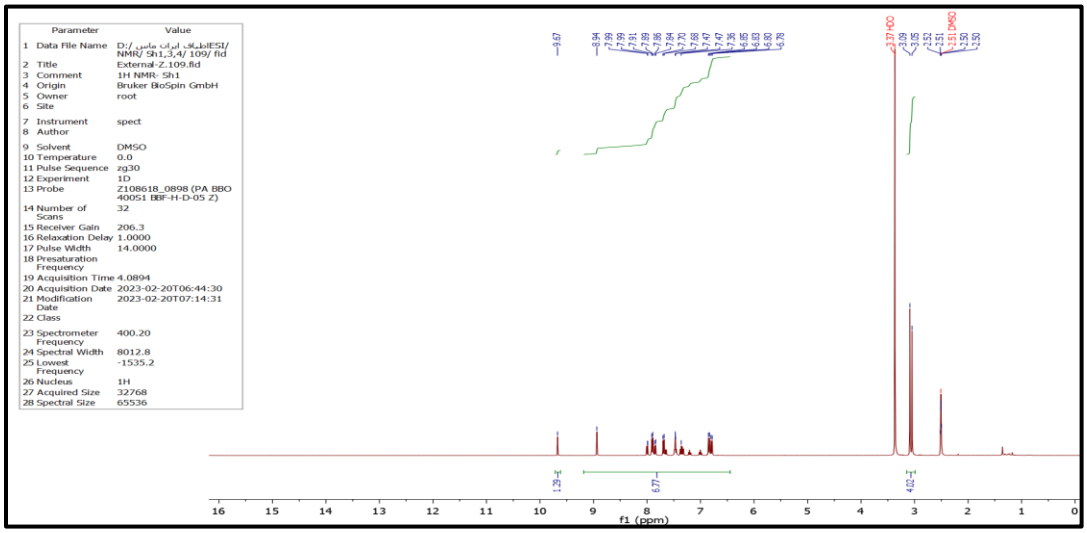

Figure 4. ^{1}H NMR spectrum of the Sh_1 molecule.

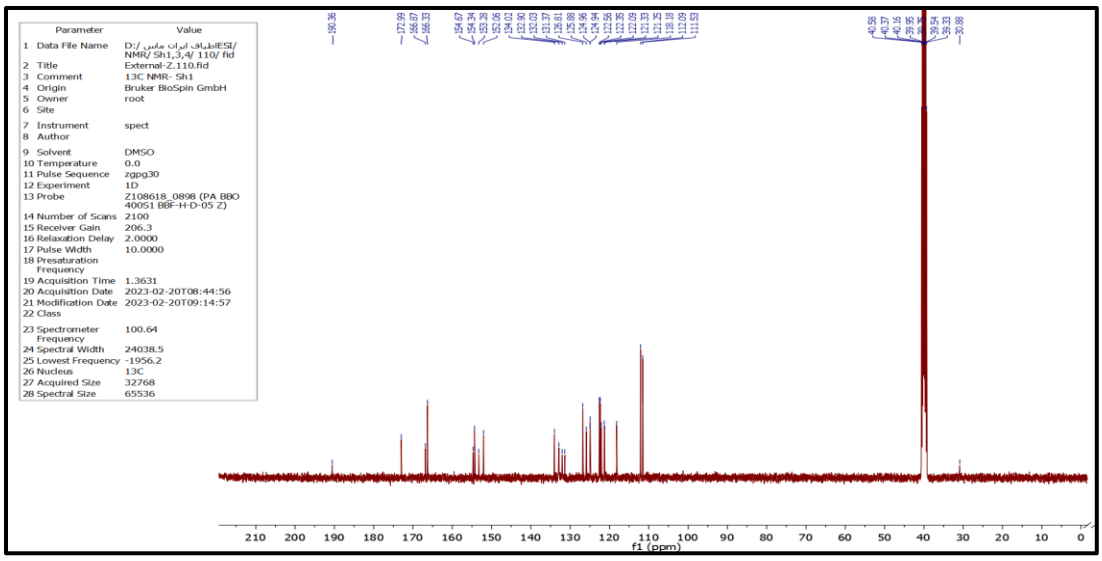

Figure 5. ^{13}C NMR spectrum of the Sh_1 molecule.

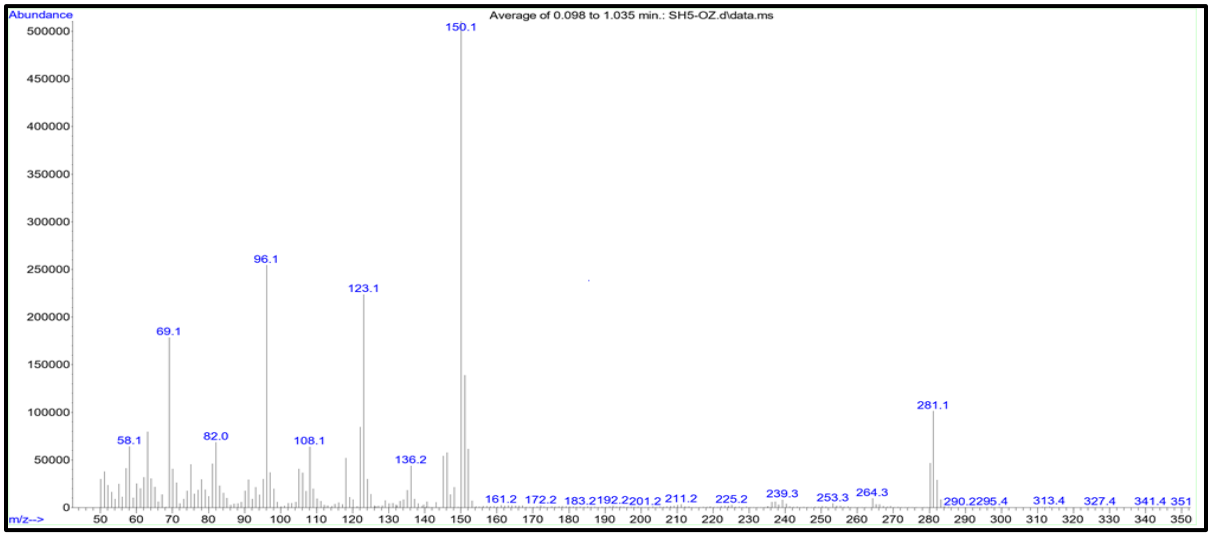

Figure 6. Sh_1 EI-Mass spectrum.

4.2. Tafel extrapolation polarization analysis

Tafel extrapolation curves were studied in 1 M of HCl. Carbon steel N80 was immersed in this solution in the absence and in the presence of various concentrations of inhibitor Sh_1, at various temperatures (298, 308, and 318 K) as shown in Figure 7(a, b and c). With an increase in the concentration of Sh_1, the corrosion potential shifts in the positive direction, while the anodic and cathodic Tafel slopes do not show a systematic change; moreover, the corrosion currents decrease. The *(%IE*) and (Θ) also increase depending on the concentration. Increasing the temperature at the same inhibitor concentration increases the corrosion current densities and decreases the inhibition efficiency [19].

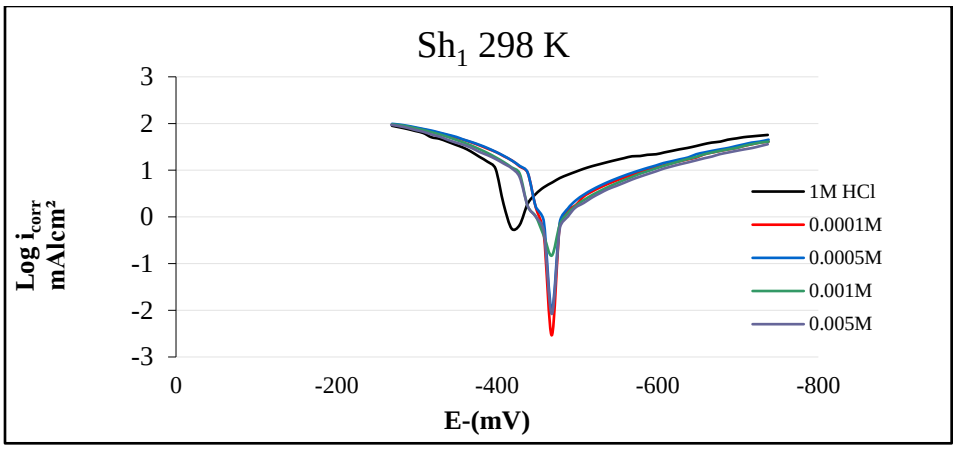

(a)

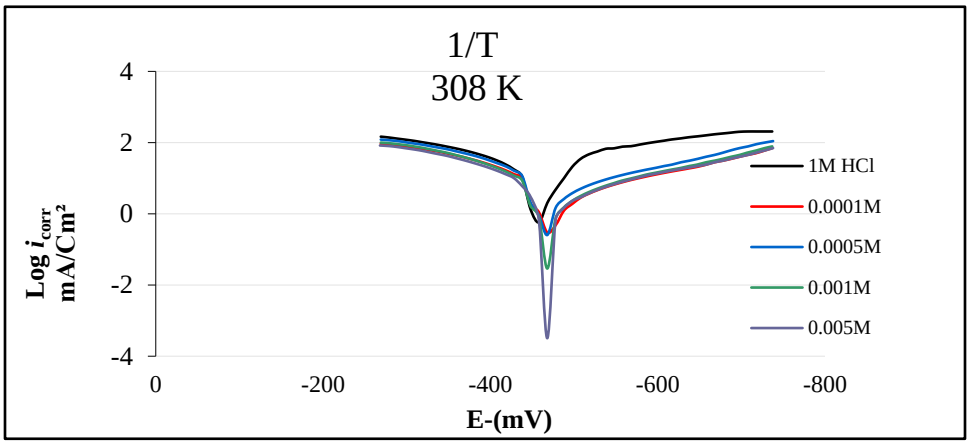

(b)

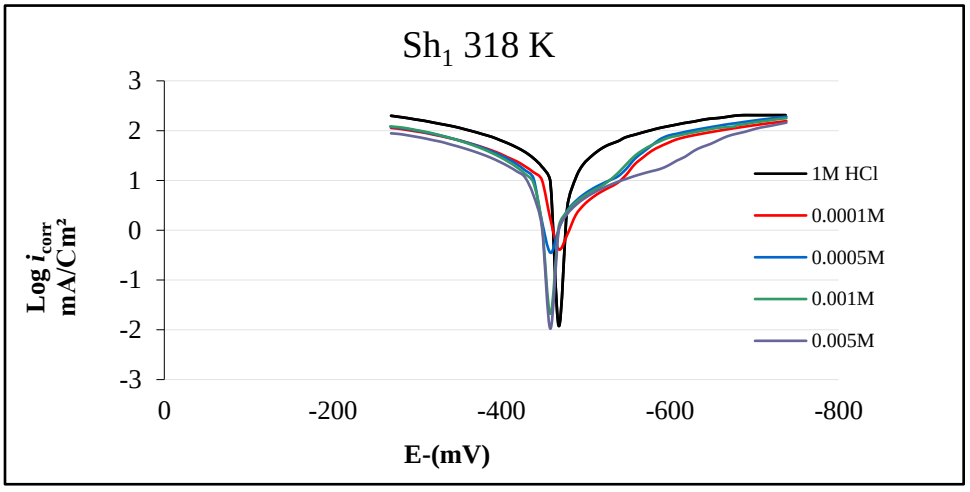

(c)

Figure 7. Tafel extrapolation polarization of steel in 1 M HCl at several temperatures (298, 308, and 318 K) at various concentrations of Sh_1 inhibitor.

Table 1 gives information about the measured variable values, including i_{corr} (corrosion current density), E_{corr} (corrosion potential), β_a (anodic slope), β_c (cathodic slope) of the Tafel curves, %*IE* = inhibition effectiveness percentage, and θ (surface coverage). This technique indicates that the iron dissolution reaction is stopped by the inhibitor, which is evident when the current density of both the anode and cathode Tafel slopes decreases. The formation is due to an adsorbent layer formed from Sh_1 on the surface of the metal that prevents the attack of the acid medium on it [20]. The electrochemical polarization measurements showed that both cathodic and anodic current densities decreased as the inhibitor concentrations increased. The findings indicate that the [%*IE*] increases with increasing concentration and temperature. Moreover, the best %*IE* = (95.71%) was provided by Sh_1 at 0.005 M and 318 K, Table 1. The surface coverage (Θ) with the layer, as well as the percentage of inhibiting effectiveness (%*IE*), are calculated using Eqs. 1 [21] and 2 [22], respectively.

$$\Theta = \frac{i^0_{corr} - i_{corr}}{i^*_{corr}} \quad (1)$$

$$\%IE = \theta \times 100 \quad (2)$$

This study investigates the corrosion current densities for the inhibited (i_{corr}) and uninhibited (i^0_{corr}) medium. Additionally, as the temperature exceeds 298 K, the (*%IE*) increases at various concentrations. The anodic current density shows little variation in the presence of the inhibitor, while the cathodic current density is significantly affected [23].

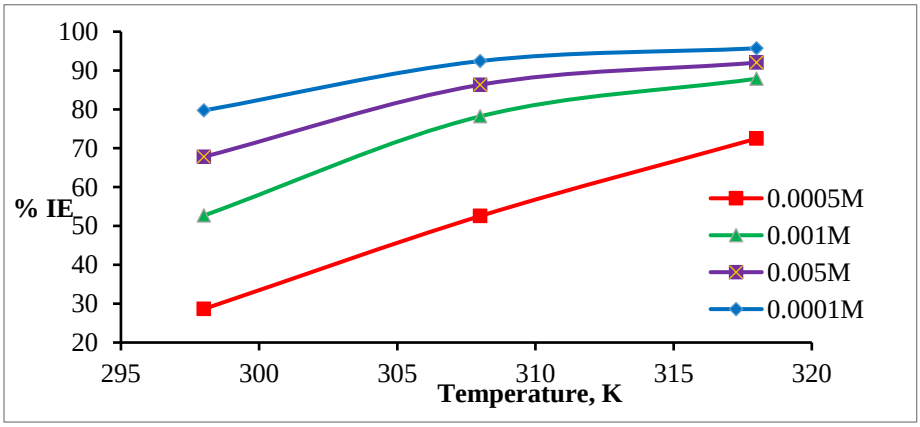

Figure 8. The effect of temperature on the inhibition efficiency percentage (%*IE*) at various inhibitor concentrations.

4.3. Effect of temperature on the inhibition efficiency percentage and corrosion rate

The temperature's impact on the corrosion rate of carbon steel N80 in 1 M HCl and the Sh_1 inhibition efficiency was examined using the Tafel polarization curves shown in Figure 8. The linear plots compare four concentrations in terms of effectiveness percentage between 298–318 K. Overall, the %IE increases with increasing temperature and concentration. Also, the corrosion rate increases with increasing temperatures but decreases with increasing

because of the increased adsorption of inhibitors on the metal surface. The greatest %*IE* in the 72–95.7% range is acquired at an optimum concentration (0.005 M) at 318 K [24], as shown in Table 1.

Table 1. Tafel extrapolation polarization measurement parameters for blank (HCl) and Sh_1 inhibited solutions at 298–318K.

Temp. [K]	Conc. of inhibitor [M]	E_{corr} –[mV]	i_{corr} [mA/cm^2]	β_c [mV/Dec]	β_a [mV/Dec]	CR [mpy]	*%IE*	Θ
298	Blank (HCl)	426.8	5.03	–235	84.2	2.29	–	–
308		469.3	14.27	–148	159.3	6.50	–	–
318		468.2	31.03	–210	207.7	14.13	-	-
298	0.0001	468.6	3.59	–249	100.7	1.63	28.62	0.28
308		469.0	6.57	–270	92.3	2.99	52.55	0.52
318		469.1	8.54	–162.4	106.9	3.88	72.47	0.72
298	0.0005	467.8	2.38	–178.3	72.6	1.08	52.68	0.52
308		468	3.11	–156.4	73.3	1.41	78.2	0.78
318		458.7	3.76	–161.6	69.8	1.71	87.88	0.87
298	0.001	468.8	1.62	–154.3	73	0.73	67.79	0.67
308		468.5	1.95	–142.5	65.8	0.88	86.33	0.86
318		458.6	2.47	–109.1	50.1	1.12	92.03	0.92
298	0.005	466.8	1.02	–130.3	63	0.46	79.72	0.79
308		468.3	1.08	–111.1	64.9	0.49	92.43	0.92
318		457.8	1.33	–81.1	49.5	0.6	95.71	0.95

4.4. Determination of activation energy (E_A)

From Arrhenius equation (Eq.3) we plot the lg i_{corr} *vs.* 1/*T* relationship (Figure 9). This equation extracts the activation energy (E_A) from the slope (straight line).

$$\mathrm{Log}\, i_{corr} = \mathrm{Log}\, A - \frac{E_A}{2.303RT} \quad (3)$$

i_{corr}, *A*, E_A, *R*, and *T* represent each the corrosion current density, the pre-exponential factor (the number of collisions in the inhibitor molecules), activation energy, universal gas constant = 8.314 J K^{-1} mol^{-1}, and temperature in Kelvin, respectively. From it, we deduce the slope value, which is $\frac{E_A}{2.303RT}$, and its intercept is Log *A* [25].

From Table 2**,** we observe that the activation energy (E_A) is reduced with an increase in inhibitor concentration because of the inhibitor molecules' gradual adsorption on carbon

steel N80. As a result, the experiment at higher temperatures approached equilibrium more closely [26]. We also note that the number of collisions of the inhibitor molecules decreases with increasing concentration, indicating that chemical adsorption of the inhibitor molecules occurs on the surface of carbon steel N80.

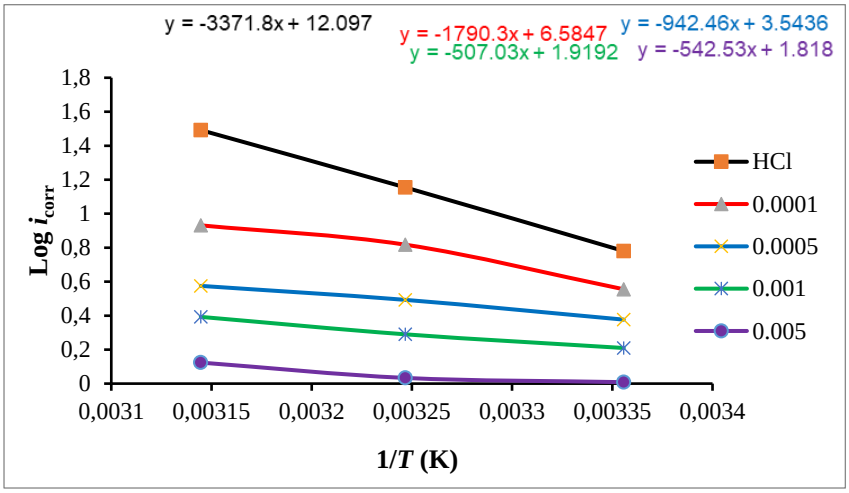

Figure 9. Arrhenius relationship in the absence and with inhibitor (Sh_1) on carbon steel N80 for a range of temperatures (298, 308, and 318 K).

Table 2. Activation energy (E_A) and pre-exponential factor (A) values in the absence and with the inhibitor.

Compound	Conc. (M)	E_A (kJ/mol)	Pre-exponential factor (A)
Blank (HCl)	1	64.56	$12.50 \cdot 10^{11}$
Sh_1 inhibitor	0.0001	34.28	$38.43 \cdot 10^{5}$
	0.0005	18.05	$34.96 \cdot 10^{2}$
	0.001	16.59	$12.96 \cdot 10^{2}$
	0.005	10.39	65.76

4.5. Adsorption isotherm

To comprehend the corrosion inhibition mechanism and the inhibitor molecules' adsorption behaviour on mild steel N80 surface, the Tafel extrapolation plot [27] was used to calculate data on the surface coverage (Θ) at various inhibitor concentrations. The data was utilized to select the optimal isotherm for estimating the adsorption technique. The validity of the results was graphically demonstrated by comparing them to different isotherms at various temperatures (298, 308, and 318 K). The relationship between the experimental findings and the isotherm is derived using Langmuir's adsorption isotherm equation [28, 29]. Accordingly, the Langmuir adsorption model assumes reversible physisorption on an energetically homogeneous adsorbent due to Van der Waals forces, according to Eq. 4.

$$\frac{C}{\theta} = \frac{1}{K_{ads}} + C \tag{4}$$

where C denotes the concentration of inhibitor, Θ is the surface coverage, and K_{ads} denotes the metal-inhibitor interaction equilibrium constant. As seen in Figure 10, a linear plot was obtained in the C/Θ *vs*. C coordinates, and K_{ads} from the intercept data represents the metal–inhibitor interaction. Subsequently, Eq. 5 was used to ascertain typical changes in free energy ΔG^0_{ads} due to adsorption.

$$\Delta G^0_{ads} = RT \ln(K_{ads} \times 55.5) \tag{5}$$

where R, T, and K refer to the universal gas constant, absolute temperature, and equilibrium constant, respectively; 55.5 denotes the molar concentration of water in solution in mol/L. The results were used to determine the spontaneity and stability of the adsorption process on the surface of carbon steel N80. The negative values of ΔG^0_{ads} supports the adsorption spontaneity and adsorbed layer's stability. Typically, ΔG^0_{ads} values up to or equal to –20 kJ/mol indicate physisorption, while values up to or equal to –40 kJ/mol indicate chemisorption [30, 31]. The value of ΔG^0_{ads} from this experiment indicates reversible physical adsorption on an energetically homogeneous adsorbent surface and electrostatic interaction. The data for the studied inhibitor is seen in Table 3.

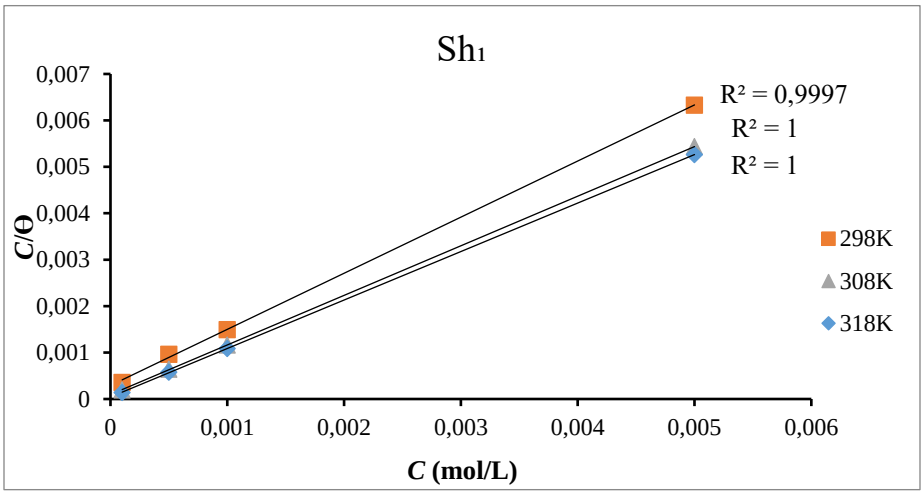

Figure 10. The Langmuir adsorption isotherm for Sh_1 inhibitor on carbon steel N80 in 1 M HCl at various temperatures.

We notice that as temperature increases, the ΔG^0_{ads} value increases. In that case, its adsorption is more favourable with a temperature increase, and this is also evidence that the inhibitor used undergoes physical adsorption on an energetically homogeneous adsorbent surface. The adsorption enthalpy ΔH^0_{ads} was calculated [32] according to Vant' Hoff formula (Eq. 6).

$$\mathrm{Log}\,K_{\mathrm{ads}} = \frac{-\Delta H_{\mathrm{ads}}}{2.303RT} + Cons \tag{6}$$

When Log K_{ads} is plotted against $1/T$, a linear line with a negative slope equal to ($-\Delta H_{ads}/2.303R$) is obtained, as illustrated in Figure 11. The thermodynamic method can estimate the entropy ΔS^0_{ads} of the Sh_1 inhibitor (Eq. 7).

$$\Delta G^0_{\mathrm{ads}} = \Delta H^0_{\mathrm{ads}} - T\Delta S^0_{\mathrm{ads}} \tag{7}$$

Based on the literature [33, 34], if ΔH^0_{ads} is negative, thermal transmission to the environment occurs during adsorption, indicating an exothermic reaction, and can either occur physically, chemically, or both. Conversely, if ΔH^0_{ads} is positive, the heat transfer occurs from the medium to the system, indicating the endothermic nature of the reaction and the chemical adsorption process. Also, the value of ΔH bigger than 100 kJ/mole corresponds to chemical adsorption. In contrast, the ΔH values smaller than 100 kJ/mol means physical adsorption. The study's findings suggest that the adsorption of the inhibitor is characterized by ΔH^0_{ads} value of 75.4313 kJ/mol, indicating physisorption. So, the ΔS^0_{ads} value is significant and positive, indicating this is increased in disorder upon transformation from a reactant towards the species adsorbed, which enhances adsorption on the metal surface [21, 35]

Table 3. Thermodynamic functions of Sh_1 adsorption on carbon steel N80 in 1 M HCl at various temperatures.

Temp. K	R^2	K_{ads}	Log K_{ads}	ΔG^0_{ads} **[kJ/mol]**	ΔH^0_{ads} **[kJ/mol]**	ΔS^0_{ads} **(J/mol·K^{-1})**
298	0.9997	3433.709	3.5357	–30.1217		354.2
308	1	10471.71	4.0200	–33.9878	75.4313	355.2
318	1	23227.71	4.3660	–37.1976		354.1

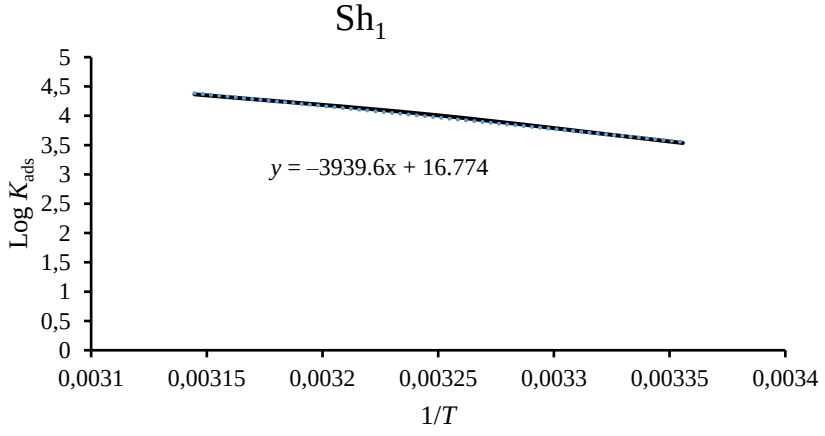

Figure 11. Correlation of Log K_{ads} *vs.* $1/T$ for carbon steel N80 in 1 M HCl solution with varying Sh_1 concentrations.

4.6. Mechanism of Sh_1 inhibition

Adsorption is enhanced by heteroatoms containing single pairs of electrons, such as N, O, S, or P, as well as π-electrons from multiple bonds or aromatic rings [36]. So, chemisorption is the process by which unbonded electrons are transferred or shared between the molecule that acts as an inhibitor and the metal's outermost layer [37]. As a result, a thin barrier coating or chemical bonds are formed due to the reaction between the inhibitor and the metal. Organic inhibitors can adsorb on metal surfaces through one of these mechanisms:

1. Attraction due to electrostatic force between charged atoms and metals.
2. Interaction of a metal surface and unpaired electrons.
3. Attraction of the metallic layer with π-electrons.

The number of locations for adsorption, the charge density, molecule size, manner of contact with the metal surface, and ability to create an insoluble metal complex all contribute to a corrosion inhibitor's performance in preventing carbon steel corrosion in a corrosive environment. The bond across the molecules that inhibit the external layer of mild steel is caused by the electrons at the double-bonded molecules and the electrons that are free on the oxygen and nitrogen particles, creating chemical bonds with the metal's outermost layer [38], as illustrated in Figure 12**.**

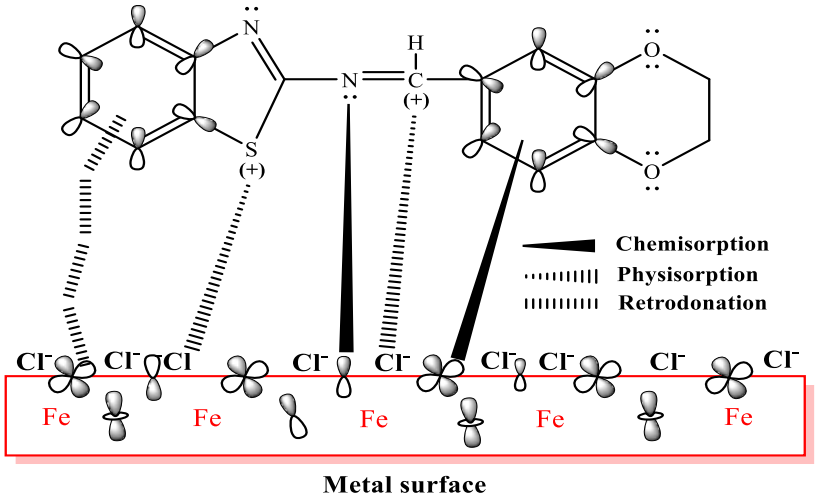

Figure 12. Adsorption mechanism for Sh_1 inhibitor on the metal surface.

4.7. Scanning electron microscopy (SEM) and energy-dispersive X-ray spectroscopy (EDS) analysis

The surface morphology of the metal was analyzed using SEM following contact in 1 M HCl and Sh_1 for approximately three hours. Figure 13 (a) shows that the newly polished mild steel surface appears smooth. However, as depicted in Figure 13 (b), the surface of the mild steel exhibits clefts and a bumpy texture due to the corrosive effects of 1 M HCl. On the other hand, Figure 13 (c) illustrates the smooth surface of the specimen without any

observable corrosion or holes in the presence of Sh_1. It suggests that Sh_1 builds a shielding barrier on the surface of mild steel, preventing corrosion. This research aims to determine the components for compounds produced in the outermost layer of metal in 1 M HCl with and without Sh_1. After that, the *EDS* chart analysis of the sites identified in SEM photos for Figures 13 (b) and (c) is displayed in Figures 14 (a) and (b). Consequently. Percentages of atomic elements found throughout the outer layer alloy from *EDS* images on rusted surfaces are 10.70% O, 3.02% Cl, 4.24% C, and 70.22% Fe. It denotes the corrosion of mild steel N80 due to the formation of iron oxide on the face of the alloy's layer. Likewise, the elemental composition acquired in the presence of Sh_1 (1.97% O, 0.44% Cl, 5.42% C, and 77.79% Fe) confirms the creation of an inhibitor barrier in this zone [39, 40]

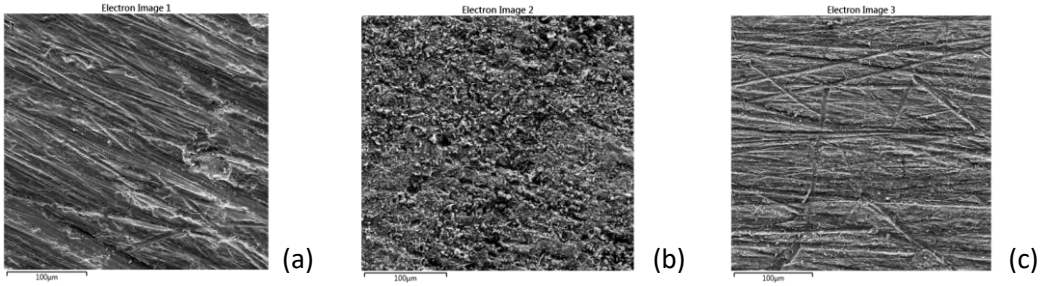

Figure 13. SEM photos of mild steel N80: (a) specimen surface polished before immersion; (b) after exposure to 1 M HCl solution; (c) after exposure to 1 M HCl solution containing 0.005 M of Sh_1 inhibitor.

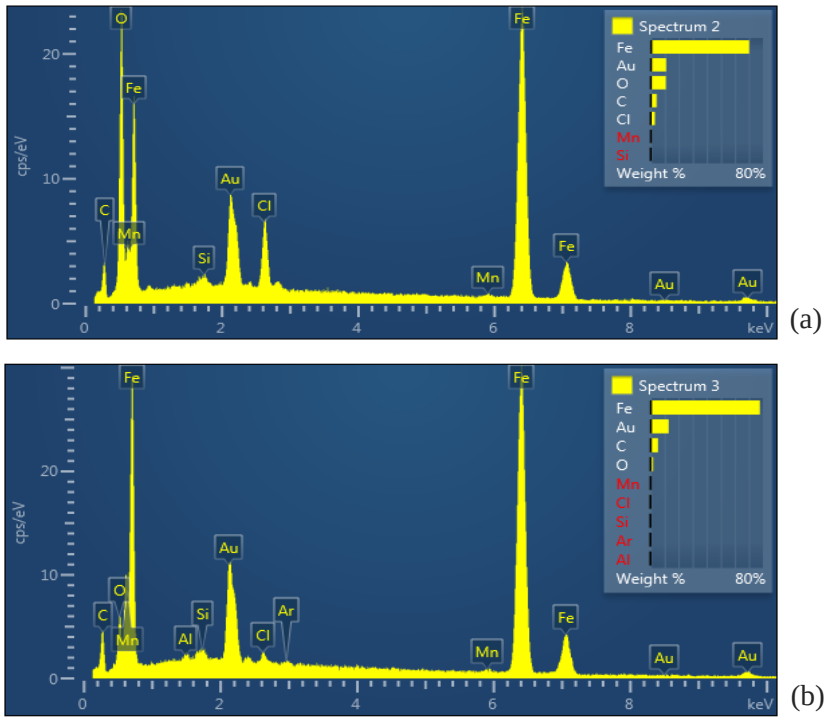

Figure 14. EDX spectrum of mild steel N80 following contact with various solutions: (a) spectrum of the specimen surface subjected to 1 M HCl solution; (b) spectrum of the specimen surface subjected to 1 M HCl solution containing 0.005 M of Sh_1 inhibitor.

Conclusion

The results of the study on the Sh_1 compound demonstrated its effectiveness in controlling carbon steel corrosion in an acidic medium, with an ultimate inhibition efficiency of 95.71% at a concentration of 0.005 M and a temperature of 318 K as determined by the potentiodynamic polarization method. The adsorption ability of Sh_1 inhibitor on surfaces of metals obeys the Langmuir equation. It is a physisorption type inhibitor, as determined by evaluation of various thermodynamic data and analysis of the adsorption isotherm. The surface morphology and EDS X-ray spectroscopy study further confirm that the inhibition activity of Sh_1 occurs via its adsorption on the metal surface.

Acknowledgment

We appreciate the cooperation of the Deanship of the College of Education for Pure Sciences at the University of Basrah. We also appreciate the assistance of the Head of the Chemistry Department at the College of Education for Pure Sciences at the University of Basrah for facilitating many of the obstacles that accompanied this work.

Authors' Declaration

Conflicts of Interest: None.
We hereby confirm that all the Figures and Tables in the manuscript are ours.
Ethical Clearance: The project was approved by the local ethical committee at the University of Basrah.

Authors' Contribution Statement

Abeer Mohammed Jabbar participated in the following roles: conducting and following up all reactions, measuring spectra of the prepared compound, and following the corrosion measurements of the prepared compound.
Adnan Sultan Abdulnabi participated in the following roles: help in interpretation of the spectral data of the prepared compound, corrosion measurements of the prepared compound, the interpretation of their results, manuscript review, and proofreading.

References

1. F. EL-Hajjaji, E. Ech-chihbi, R. Salim, A. Titi, M. Messali, B. El Ibrahimi, S. Kaya and M. Taleb, A detailed electronic-scale DFT modeling/MD simulation, electrochemical and surface morphological explorations of imidazolium-based ionic liquids as sustainable and non-toxic corrosion inhibitors for mild steel in 1 M HCl, *Mater. Sci. Eng.: B*, 2023, **289**, 116232. doi: 10.1016/j.mseb.2022.116232
2. E. Ech-chihbi, R. Salim, H. Oudda, A. Elaatiaoui, Z. Rais, A. Oussaid, F. El Hajjaji, B. Hammouti, H. Elmsellem, M. Taleb, Effect of some imidazopyridine compounds on carbon steel corrosion in hydrochloric acid solution, *Der Pharma Chem.*, 2016, **8**, no. 13, 214–230.

3. A.A. Al-Amiery, W.N.R.W. Isahak and W.K. Al-Azzawi, Corrosion Inhibitors: Natural and Synthetic Organic Inhibitors, *Lubricants*, 2023, **11**, no. 4, 174. doi: 10.3390/lubricants11040174
4. A. Ahmed, A. Abdul, M. Abdul Hameed, M. Abu Bakar and S. Pua, Novel Corrosion Inhibitor for Mild Steel in HCl, *Materials*, 2014, **2**, 7, 662–672. doi: 10.3390/ma7020662
5. I. Taleb, G. Elron, B. Ime, K. Mustafa and A. Mohamed, Corrosion inhibition of mild steel by Calotropis procera leaves extract in a CO_2 saturated sodium chloride solution, *J. Adhes. Sci. Technol*., 2016, **23**, no. 30, 2523–2543. doi: 10.1080/01694243.2016.1185229
6. C. Marko and C. Fidelis, Recent Natural Corrosion Inhibitors for Mild Steel: An Overview, *J. Chem*., **2016**, 2016, 1–7. doi: 10.1155/2016/6208937
7. Q. Dinh, D. Tran, C. Pham, Effect of the Structure and Temperature on Corrosion Inhibition of Thiourea Derivatives in 1.0 M HCl Solution, *ACS Omega*, 2019, **11**, no. 4, 14478–14489. doi: 10.1021/acsomega.9b01599
8. R. Salim, A. Nahlé, F. El-Hajjaji, E. Ech-chihbi, F. Benhiba, F. El Kalai, N. Benchat, H. Oudda, A. Guenbour, M. Taleb and I. Warad, Experimental, density functional theory, and dynamic molecular studies of imidazopyridine derivatives as corrosion inhibitors for mild steel in hydrochloric acid, *Surf. Eng. Appl. Electrochem*., 2021, **57**, no. 2, 233–254. doi: 10.3103/S1068375521020083
9. B.C. Sahu, *Organic Corrosion Inhibitors*, IntechOpen, 2023. doi: 10.5772/intechopen.109523
10. D.S. Zinad, M. Hanoon, R.D. Salim, S.I. Ibrahim, A.A. Al-Amiery, M.S. Takriff and A.A.H. Kadhum, A new synthesized coumarin-derived Schiff base as a corrosion inhibitor of mild steel surface in HCl medium: gravimetric and DFT studies, *Int. J. Corros. Scale Inhib*., 2020, **9**, no. 1, 228–243. doi: 10.17675/2305-6894-2020-9-1-14
11. Prakash Shetty, Schiff bases: An overview of their corrosion inhibition activity in acid media against mild steel, *Chem. Eng. Commun*., 2020, **207**, no. 7, 985–1029. doi: 10.1080/00986445.2019.1630387
12. A. El Yaktini, A. Lachiri, M. El Faydy, F. Benhiba, H. Zarrok, M. El-Azzouzi, M. Zertoubi, M. Azzi, B. Lakhrissi and A. Zarrouk, Inhibitor effect of new azomethine derivative containing an 8-hydroxyquinoline moiety on corrosion behavior of mild carbon steel in acidic media, *Int. J. Corros. Scale Inhib*., 2018, **7**, no. 4, 609–632. doi: 10.17675/2305-6894-2018-7-4-9
13. A.M. Jabbar and A.S. Abdulnabi. Effect of organic corrosion inhibitors functional groups (azo and azomethine) on carbon steel N80 alloy corrosion using the electrochemical polarization technique, *Int. J. Corros. Scale Inhib*., 2024, **13**, no. 1, 165–183. doi: 10.17675/2305-6894-2024-13-1-9

14. S. Garima and S. Manjul, Microwave Assisted Synthesis and Characterization of Schiff Base of 2-Amino Benzimidazole, *Int. J. Pharm. Sci. Drug Res*., 2018, **10**, no. 4, 293–296. doi: 10.25004/IJPSDR.2018.100414
15. M.Y. Tabarek and M.A. Ahlam, Synthesis and Characterization of New Bis-Schiff Bases Linked to Various Imide Cycles, *J. Sci*., 2023, **64**, no. 3, 1062–1070. doi: 10.24996/ijs.2023.64.3.3
16. H. Qusay and Z. Dakhil, Study of the Anticancer and Antimicrobial Biological Activity of a New Series of Thiohydantoin Derivatives, *J. Sci*., 2023. doi: 10.21123/bsj.2023.7978
17. N.E. Felicia, O.R. Mujeeb, A.O. Oluwakemi and M.F. Tolulope, Schiff bases as analytical tools: synthesis, chemo-sensor, and computational studies of 2-aminophenol Schiff bases, *Mat. Adv*., 2023, **10**, no. 4, 2308–2321. doi: 10.1039/d3ma00097d
18. J. Sara, K. Dmytro, J. Michał, K. Urszula, S. Paulina, S. Marta and W. Monika, Synthesis and Biological Evaluation of New Schiff Bases Derived from 4-Amino-5-(3-fluorophenyl)-1,2,4-triazole-3-thione, *Molecules*, 2023, **28**, no. 6, 2718. doi: 10.3390/molecules28062718
19. M. Şahin, S. Bilgiç and G. Gece, Inhibition of Armco iron corrosion in 1 M HCl medium using saponin: Experimental and computational studies, *Int. J. Corros. Scale Inhib*., 2020, **9**, no. 4, 1444–1458. doi: 10.17675/2305-6894-2020-9-4-16
20. S. Zahra, P. Mahmoud, A. Abbas and R. Rahim, Hybrid graphene oxide decoration and water-based polymers for mild steel surface protection in saline environment, *J. Ind. Eng. Chem*., 2019, **74**, 41–54. doi: 10.1016/j.jiec.2019.01.043
21. Z. Abdelkader, A. Salem, H. Hanane, D. Tahar, A. Mousa and G. Noureddine, Molecular dynamic simulation and experimental investigation on the synergistic mechanism and synergistic effect of (1Z) *N* [2 (methylthio) phenyl] 2oxopropanehydrazonoyl chloride (S1) corrosion inhibitor on mild steel in acid medium 1 M HCl, *J. Ind. Eng. Chem*., 2023, **100**, 100832. doi: 10.1016/j.jics.2022.100832
22. H. Mazin, K. Noor Ali, H. Taghreed, R. Salam, H. Hussian and M. Shatha, Enhancement of corrosion protection of metal carbon steel C45 and stainless steel 316 by using inhibitor (Schiff base) in seawater, *J. Sci*., 2022, **20**, no. 3, 1012–1026. doi: 10.21123/bsj.2023.7749
23. A. Ehteram, Noor, Temperature Effects on the Corrosion Inhibition of Mild Steel in Acidic Solutions by Aqueous Extract of Fenugreek Leaves, *Int. J. Electrochem. Sci*., 2007, **2**, 996–1017. doi: 10.1016/S1452-3981(23)17129-X
24. P.P. Kumari, P. Shetty, A. Suma, Electrochemical measurements for the corrosion nhibition of mild steel in 1 M hydrochloric acid by using an aromatic hydrazide derivative, *Arab. J. Chem*., 2017, **10**, no. 5, 653–663. doi: 10.1016/j.arabjc.2014.09.005
25. L.C. Go, D. Depan, W.E. Holmes, A. Gallo, K. Knierim, T. Bertrand and R. Hernandez, Kinetic and thermodynamic analyses of the corrosion inhibition of synthetic extracellular polymeric substances, *J. Mat. Sci*., 2020, **2**, 1–22. doi: 10.7717/peerj-matsci.4

26. O.A. Akinbulumo, O.J. Odejobi and E.L. Odekanle, Thermodynamics and adsorption study of the corrosion inhibition of mild steel by Euphorbia heterophylla L. extract in 1.5 M HCl, *Results Mater*., 2020, **5**, 100074. doi: 10.1016/j.rinma.2020.100074
27. S. Osami and S. Burapornpong, The Differentiating Polarization Curve Technique for the Tafel Parameter Estimation, *Catalysts*, 2017, **7**, 239. doi: 10.3390/catal7080239
28. V. Sheeja and S. Subhashini. Pavetta Indica Bark as Corrosion Inhibitor in Mild Steel Corrosion in HCl and H_2SO_4 Medium: Adsorption and Thermodynamic Study, *Chem. Sci. Trans*., 2014, **3**, no. 1, 129–140, doi: 10.7598/cst2014.656
29. H. Hanane, D. Tahar, D. Djamel, A. Mousa and C. Salah, Corrosion inhibition efficiency and adsorption behavior of azomethine compounds at mild steel/hydrochloric acid interface, *Measurement*, 2016, **94**, 837–846. doi: 10.1016/j.measurement.2016.09.027
30. T. Hadi, Y. Mouayed and S. Adnan, Quantum Chemical Calculations and Experimental Studies of using Azo Dye as Corrosion Inhibitors for on Carbon Steel in Acidic Medium. *J. Adv. Res. Chem. Sci*., 2022, **2**, no. 1, 1–9. Link
31. K. Moafaq, G. Tayser Sumer, A mini review on corrosion, inhibitors and mechanism types of mild steel inhibition in an acidic environment, *Int. J. Corros. Scale Inhib*., 2021, **10**, no. 3, 861–884. doi: 10.17675/2305-6894-2021-10-3-2
32. E Khamis, The Effect of Temperature on the Acidic Dissolution of Steel in the Presence of Inhibitors, *Corrosion*, 1990, **46**, no. 2, 476–484. Link
33. D. Djamel, D. Tahar, I. Saifi and C. Salah, Adsorption and corrosion inhibition of new synthesized thiophene Schiff base on mild steel X52 in HCl and H_2SO_4 solutions, *Corros. Sci*., 2014, **79**, 50–58. doi: 10.1016/j.corsci.2013.10.025.
34. T. Mingjin, L. Jianbo, L. Zhida, F. Luoping, Z. Bo and L. Jie, Mannich Base as Corrosion Inhibitors for N80 Steel in a CO_2 Saturated Solution Containing 3 wt % NaCl, *Materials*, 2019, **12**, 449. doi: 10.3390/ma12030449
35. Z. Ammar, N. Salah, A. Salem, K. Latifa, K. Aicha, K. Abasse, A. Mousa, G. Djamel, A. Mohamed, A. Abdelmajeed and E. Noureddine, Corrosion Inhibition of Azo Compounds Derived from Schiff Bases on Mild Steel (XC70) in (HCl, 1 M DMSO) Medium: An Experimental and Theoretical Study, *ACS Omega*, 2023, **8**, 21571–21584. doi: 10.1021/acsomega.3c00741
36. G. Lei, D. Weipeng and Z. Shengtao, Theoretical challenges in understanding the inhibition mechanism of copper corrosion in acid media in the presence of three triazole derivatives, *RSC Adv*., 2014, **79**, 41956–41967. doi: 10.1039/C4RA04931D
37. G. Lei, Q. Chengwei, Z. Xingwen, Z. Renhui, S. Xun, K.S. Sava, Toward understanding the adsorption mechanism of large size organic corrosion inhibitors on an Fe(110) surface using the DFTB method, *RSC Adv*., 2017, **7**, 29042. doi: 10.1039/c7ra04120a
38. A.K. Alamry, A.M. Hussein, A. Musa, K. Haruna and A.T. Saleh, The inhibition performance of a novel benzenesulfonamide-based benzoxazine compound in the corrosion of X60 carbon steel in an acidizing environment, *RSC Adv*., 2021, **11**, 7078–7095. doi: 10.1039/D0RA10317A

39. A. Solé, C. Barreneche, I. Martorell and L.F. Cabeza, Corrosion evaluation and prevention of reactor materials to 2 contain thermochemical material for thermal energy storage, *Appl. Therm. Eng*., 2015, **16**, 21. doi: 10.1016/j.applthermaleng.2015.10.156
40. B. Said, C. Omar and E. Ahmed, Synthesis of a New Asymmetric Composite Membrane with Bi-Component Collodion: Application in the Ultra filtration of Baths of Reagent Dyes of Fabric Rinsing/Padding, *J. Mater. Environ. Sci*., 2016, **7**, no. 12, 4556–4569. Link

♦ ♦ ♦